A Self-Organizing Global Sliding Mode Control and Its Application to Active Power Filter

Shixi Hou and Juntao Fei, *Senior Member, IEEE*

***Abstract*—In this article, a self-organizing global sliding mode control (GSMC) is developed for a class of dynamic systems, whereby modeling uncertainties are estimated by metacognitive fuzzy-neural-network (MCFNN) framework. First, a GSMC is designed for the tracking of reference signals to eliminate the reaching mode and chattering phenomenon. To overcome the drawbacks of GSMC, the control law is designed based on MCFNN instead of the uncertain information. Distinguished from the fixed structure schemes, MCFNN can restructure the network structure and parameters by extracting useful input data not all data. Moreover, in order to alleviate redundant or inefficient computation, only the parameters of the rule nearest to the current data instead of all rules are updated online based on Lyapunov stability analysis. Finally, simulation and experimental investigations on active power filter are employed to verify the control performance of proposed controller.**

***Index Terms*—Active power filter (APF), adaptive control, fuzzy neural network (FNN), sliding mode control (SMC).**

I. Introduction

IN PRACTICAL applications, various kinds of disturbances and uncertainties adversely affect the performance of control systems, which make the control design difficult. In recent decades, many types of control strategies have been developed for nonlinear dynamic systems [1], [2]. Due to its robustness to system uncertainties, sliding mode control (SMC) has been one of the most widely and efficiently utilized control schemes for uncertain systems [3]–[5]. There are two different modes, namely reaching mode and sliding mode, in the traditional SMC. It is worth mentioning that the insensitive to parameter variations and external disturbances exists only in the sliding mode phase. That is, there is no global robustness in the traditional SMC. Under these circumstances, the concept of global sliding mode control (GSMC) method is proposed to offer a general structure to eliminate the reaching phase [6]. In GSMC, by using an extra term in the switching curve, the reaching interval of SMC is removed and the states move on the switching curve exactly from the beginning [7], [8]. GSMC can guarantee the robustness and acceleration of the system and remove the reaching phase, such that it has been successfully applied to various practical systems [9], [10]. Inspired by the superior benefits of the GSMC technique, we thus apply the GSMC control approach to realize the tracking issue in this article and experimentally evaluate its remarkable performance.

However, there are some problems to be solved for GSMC, such as chattering phenomena, requirement of prior knowledge. It should be noted that chattering phenomenon could cause IGBT malfunction to deteriorate power quality. Using quasi-SMC, first one can be overcome in which conventional-SMC is adopted only in the boundary layer outside, whereas continuous state feedback control is executed in the boundary layer to eliminate the chattering [11]. And one of the effective approaches to relax the dependence on prior knowledge of GSMC is uncertainty observer. Different from other typical state observer like Luenberger observer and adaptive observers [12]–[15] which require the exact model information, intelligent control-based estimators behaves with a very strong robustness due to an inherent ability to learn and approximate a nonlinear function [16], [17]. In general, in order to relax the dependence on system information, intelligent control such as fuzzy SMC and neural network SMC [18]–[20] were further developed in two ways. One is to estimate the bounds of uncertainties in Lyapunov framework so that the stability of closed-loop system can be ensured, while the other is to design an uncertainty observer for directly learning the unknown function. Over the past decades, fuzzy neural network (FNN) system has drawn more and more attention due to its combined advantages in fuzzy logic and neural network. Therefore, FNN have been developed for uncertain nonlinear systems in the control design [21]–[23].

It is noteworthy that all of the above FNN control methods are developed only considering parameter learning with predefined structure. From the perspective of practice, the generalization ability of FNN with fixed structure is actually limited especially when reference signals rapidly change [24]. In [25], [26], for eliminating harmonics in the ac electric railway systems, an APF is developed, in which discontinuity of driving frequency leads to frequent changes in traction loads. Using FNN without structure updated online, control ability would be greatly reduced if adverse fuzzy rules are defined in advance in this context. By exploiting adaptive capability of parameters and structures during

Manuscript received July 22, 2019; revised September 18, 2019 and November 7, 2019; accepted November 27, 2019. Date of publication December 4, 2019; date of current version March 13, 2020. This work was supported in part by the Natural Science Foundation of Jiangsu Province under Grants BK20170303 and BK20171198, in part by the Changzhou Sci&Tech Program under Grant CJ20190056, in part by the Fundamental Research Funds for the Central Universities under Grants 2017B03014 and 2017B20014, and in part by the National Natural Science Foundation of China under Grant 61873085. Recommended for publication by Associate Editor C. K. Tse. *(Corresponding author: Shixi Hou.)*

The authors are with the Jiangsu Key Laboratory of Power Transmission and Distribution Equipment Technology and College of IOT Engineering, Hohai University, Nanjing 210098, China (e-mail: shixi_hou@yahoo.com; johnfei123@163.com).

Color versions of one or more of the figures in this article are available online at http://ieeexplore.ieee.org.

Digital Object Identifier 10.1109/TPEL.2019.2958051

the operating process, self-organizing FNN has been applied for nonlinear dynamic system to improve the generalization capabilities of FNN [27]–[30]. Since metacognitive algorithms possess the advantages to handle optimization problems, structural adaptive ability can be realized using metacognitive fuzzy neural network (MCFNN) [31], [32]. In the MCFNN, fuzzy rules and number of nodes both are not predefined at the beginning, and the structure and network parameters will be adjusted with data deletion and learning schemes to realize a full learning process.

In this article, a self-organizing global sliding mode control (SOGSMC) is proposed to design a high-performance control system for a class of dynamic systems. Quasi-GSMC is constructed to impose robustness, eliminate reaching phase, and avoid chattering phenomenon. In addition, MCFNN is combined to quasi-GSMC to relax the requirement of system information. The novel control law can be easy to be implemented due to low computation burden. The closed-loop stability and zero convergence of tracking errors can be achieved by Lyapunov analysis. The major contributions of this article are summarized as follows:

1) Due to system uncertainties and unknown external disturbances, an MCFNN control with structure adjustment online is given to estimate unknown functions. The MCFNN could realize more complex function fitting and higher mimicking accuracy by fast convergence using evolving parameters and structure. Its superiority is to increase the control accuracy and decrease the response time for dynamic systems.
2) MCFNN is introduced to provide with a good estimate for unknown terms of dynamic system because of unexpected perturbations in practical systems. Only if current input variables meet the requirements of data learning scheme, parameter updating mechanism will be triggered. In this way, computational burden is reduced for real-time control. In data learning scheme, hidden nodes and fuzzy rules can be generated or deleted based on the measurement of current input variable.
3) As it is difficult to establish accurate mathematical model for dynamic systems because of their nonlinearity and uncertainties, an SOGSMC which possess the salient merit of robust control has a great potential for a class of dynamic systems. Simulation and experimental results also showed that the proposed controller could achieve satisfactory performance.

Remark 1: The GSMC has been introduced for various nonlinear systems. For example, in [7], a GSMC is presented for active power filter (APF). But the requirements of detailed system information limit its applications. For most practical systems, the unpredictable perturbations always exist, which have adverse effects on the control performance. It is noteworthy that most of the system parameters except for the constant term B are not needed in the proposed controller (29). In recent years, fuzzy system and neural network is utilized to estimate unknown function. However, it is noteworthy that it is a challenge to handle the definite inference mechanism in the neural network, and it is difficult for engineers to choose suitable membership functions in the fuzzy system. MCFNN not only possess the merits of the humanoid reasoning and parameter adaptive ability, but also reveal better learning abilities with structural adjustment compared with the FNN with fixed structure in [23]. In addition, distinguish from the existing work [23], metacognitive schemes including data deletion and data learning can be executed concurrently online in the proposed control method. The input variables under the requirements of data learning are deleted and not trigger the parameter updating mechanism, which avoids the over-learning and enhance the generalization capability in real-time control. Data learning scheme aims to achieve determining the network structure and adjusting parameters simultaneously. All of the membership functions are automatically added into rule base online. Moreover, different from the existing GSMC susceptible to chattering phenomenon aroused by the sign function, the proposed control law is softened using the designed boundary layer and chattering problem can be attenuated effectively. Thus, this study aims to propose a GSMC-based MCFNN control strategy to realize accurate, smooth, and reliable control. In addition, network parameters of the proposed control scheme are online updated derived from Lyapunov stability theorem to assure the convergence ability and stable control performance. In the state of the art, there is no GSMC using MCFNN that reliable control and system stability can be realized contemporaneously for dynamic systems with unknown lumped uncertainties. Therefore, the main novelty of this study is that GSMC using MCFNN is introduced to ensure better control performance for dynamic systems. Moreover, GSMC using MCFNN can be implemented in various applications, such as automobile electronic throttle, surface vehicles, and hybrid maglev transportation system.

II. Problem Statement

For the simplification of illustration, consider a class of universal multiinput systems

$$\dot{X} = F(X) + BU \tag{1}$$

where $X \in R^n$ represents a state vector and $U \in R^n$ is a control input vector, $F(X) \in R^n$ is assumed to be unknown and bounded nonlinear functions, and $B \in R^{n\times n}$ is parameter matrices.

As mentioned before, parameter perturbation and external disturbance have adverse effects on practice systems, so the universal multiinput nonlinear systems should be described as

$$\dot{X} = F(X) + \Delta F(X) + (B + \Delta B)U + d \tag{2}$$

where $\Delta F(X)$ and ΔB are the uncertainties of $F(X)$ and B, d presents an unknown perturbation caused by unmodeled dynamics and external disturbance.

The system model (1) could be rewritten as

$$\dot{X} = F(X) + BU + H \tag{3}$$

where $H \in R^n$ is a lumped perturbation given by

$$H = \Delta F(X) + \Delta BU + d. \tag{4}$$

Assumption 1: The uncertainty H is bounded such that $\|H\| \le H_M$, where H_M is a known positive constant.

The conventional GSMC for (3) is described in the following part by assuming all the parameters of the system are well known.

The tracking error between the state trajectory X and reference trajectory X_d and its derivative can be defined as

$$e = X - X_d \tag{5}$$

$$\dot{e} = \dot{X} - \dot{X}_d. \tag{6}$$

The following global sliding surface can be expressed as

$$S = Ce - g(t) \tag{7}$$

where C is a positive constant, $g(t) \in R^n$, g_i is the element of the vector $g(t)$, which should be properly designed if following three conditions are satisfied:

1) $g_i(0) = ce_{i0}$,
2) If $t \to \infty$, $g_i \to 0$,
3) g_i has a first derivative.

where e_{i0} is an initial value of e_i, e_i is the element of the vector e.

So g_i can be designed as $g_i = g_i(0)\mathrm{e}^{-kt}$, where k is a constant.

The time derivative of S is

$$\begin{aligned}\dot{S} &= C\dot{e} - \dot{g}(t) \\ &= C(\dot{X} - \dot{X}_d) - \dot{g}(t) \\ &= C[F(X) + BU + H - \dot{X}_d] - \dot{g}(t).\end{aligned} \tag{8}$$

Then, the GSMC is adopted as

$$U_{gsm} = \frac{B^{-1}}{C}[\dot{g}(t) - CF(X) + C\dot{X}_d - D\mathrm{sgn}(S)] \tag{9}$$

where D is a designed positive constant.

Proof: Choose a Lyapunov function as

$$V_1 = \frac{1}{2}S^T S. \tag{10}$$

Differentiating (10) with respect to time, the following expression can be obtained:

$$\dot{V}_1 = S^T[C(F(X) + BU + H - \dot{X}_d) - \dot{g}(t)]. \tag{11}$$

Substituting the controller (9) into (11), it can be obtained that

$$\begin{aligned}\dot{V}_1 &= S^T[C(F(X) + C^{-1}(\dot{g}(t) - CF(X) + C\dot{X}_d \\ &\quad - D\mathrm{sgn}(S)) + H - \dot{X}_d) - \dot{g}(t)] \\ &= S^T[CH - D\mathrm{sgn}(S)] = -D\|S\| + S^T CH \\ &\le -D\|S\| + \|S\| CH_M = \|S\|(CH_M - D).\end{aligned} \tag{12}$$

The above inequality (12) meets $\dot{V}_1 < 0$ when $D > CH_M$. The negative definite of $\dot{V}_1$ means that V_1, S both are bounded. From (8), we can conclude that $\dot{S}$ is also bounded, and the GSMC can ensure superior trajectory tracking performance and guarantee closed-loop asymptotic stability.

However, the GSMC requires model parameters of dynamic systems, which is difficult to acquire. In this context, $F(X)$ should be termed as unknown function due to the unexpected perturbations. So the controller (9) cannot be achieved. Thus, to alleviate aforementioned problem, an MCFNN approximator is introduced in the next part. The main feature of MCFNN approximator is to use MCFNN for learning uncertain parts to realize robust control performance in Section III.

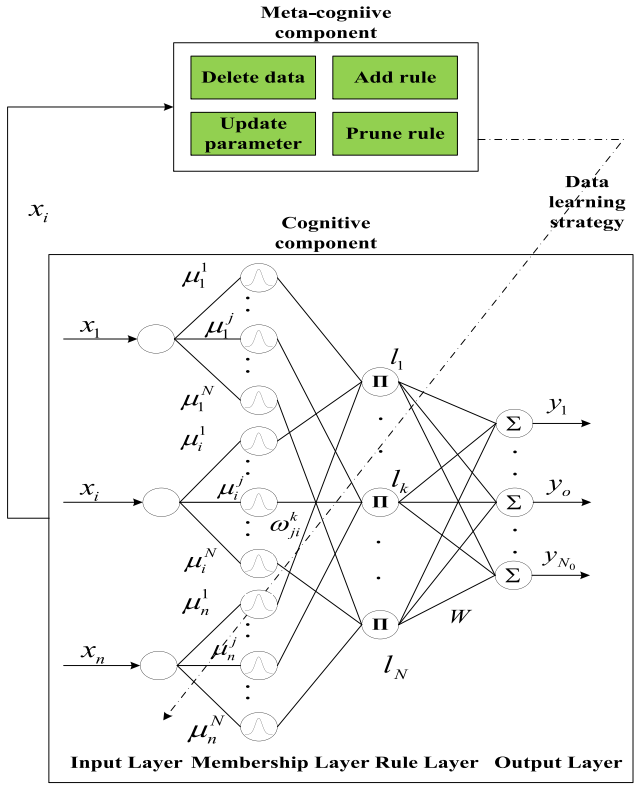

Fig. 1. Structure of MCFNN.

Remark 2: For the control law defined in (9), if the sign function $\mathrm{sgn}(s)$ is replaced by saturation function, that is

$$U_{gsm} = \begin{cases} \frac{B^{-1}}{C}\left[\dot{g}(t) - CF(X) + C\dot{X}_d - D\mathrm{sgn}(S)\right] & \text{if } \|S\| > \beta \\ \frac{B^{-1}}{C}\left[\dot{g}(t) - CF(X) + C\dot{X}_d - D\frac{S}{\beta}\right] & \text{if } \|S\| \le \beta \end{cases} \tag{13}$$

where β is a designed positive parameter, then the chattering will be reduced.

III. Metacognitive Fuzzy Neural Network (MCFNN)

A. Structure of MCFNN

For purpose of enhancing the tracking performance, relaxing the restrictions associated with GSMC, and reducing the computational complexity, the proposed MCFNN system combines cognitive component and metacognitive component in this section. The proposed MCFNN, shown in Fig. 1, is constructed by a four-layer MCFNN framework. The detailed signal propagation process of the proposed MCFNN is described as follows.

1) First Layer. Input Layer: The input layer completes the transmission of the input variables ($X = [x_1 \cdots x_i \cdots x_n]^T$).

2) Second Layer. Membership Layer: Gaussian functions are introduced to denote the signal propagation process of this layer, which can be expressed as follows:

$$\mu_i^j(x_i) = \exp\left[-\frac{(x_i - c_i^j)^2}{(b_i^j)^2}\right] \tag{14}$$

where $c_i^j (i = 1, \ldots, n, j = 1, \ldots, N)$ and b_i^j is the central vector and the base width of the Gaussian function, respectively. For every input variable x_i, the number of membership functions is N. For purpose of illustration, b and c, where all central vector and base width is collected, can be determined as

$$\begin{aligned} b &= [\, b_1 \; b_2 \; \cdots \; b_N \,]^T \\ &= \left[\, b_1^1 \; \cdots \; b_n^1 \; b_1^2 \; \cdots \; b_n^2 \; \cdots \; b_1^N \; \cdots \; b_n^N \,\right]^T \in R^{N_r \times 1} \end{aligned}$$

and

$$\begin{aligned} c &= [\, c_1 \; c_2 \; \cdots \; c_N \,]^T \\ &= \left[\, c_1^1 \; \cdots \; c_n^1 \; c_1^2 \; \cdots \; c_n^2 \; \cdots \; c_1^N \; \cdots \; c_n^N \,\right]^T \in R^{N_r \times 1} \end{aligned}$$

where $N_r = n^* N$.

3) Third Layer. Rule Layer: The input signals $\mu_i^j(x_i)$ multiplies each node k in this layer and the product becomes the output of this layer, termed as the fuzzy inference mechanism. The relationship can be denoted as

$$l_k = \exp\left[-\sum_{i=1}^{n} \frac{(x_i - c_i^j)^2}{(b_i^j)^2}\right] \tag{15}$$

where $l_k (k = 1, \ldots, N)$ denotes the kth output of this layer; N represents the total number of fuzzy rules.

4) Fourth Layer. Output Layer: Each node $y_o (o = 1, \ldots, N_o)$ in this layer sums the outputs in previous layer, which can be stated as

$$y_o = \sum_{k=1}^{N_y} \omega_k^o \cdot l_k \tag{16}$$

in which $\omega_o = [\, \omega_1^o \; \omega_2^o \; \cdots \; \omega_N^o \,]$.

Thus, the outputs of the proposed MCFNN are expressed to take the following form:

$$y = [\, y_1 \; \cdots \; y_o \; \cdots \; y_{N_o} \,]^T = Wl \tag{17}$$

where

$$W = \begin{bmatrix} \omega_1^1 & \omega_2^1 & \cdots & \omega_N^1 \\ \omega_1^2 & \omega_2^2 & \cdots & \omega_N^2 \\ \vdots & \vdots & \ddots & \vdots \\ \omega_1^{N_o} & \omega_2^{N_o} & \cdots & \omega_N^{N_o} \end{bmatrix} = \begin{bmatrix} \omega_1 & \omega_2 & \cdots & \omega_{N_o} \end{bmatrix}^T$$

$$l = \begin{bmatrix} l_1 & l_2 & \cdots & l_N \end{bmatrix}^T.$$

B. Metacognitive Learning Mechanism

Using three different strategies including data learning, data deleting, and data reserving, the structure and network parameters of MCFNN both can be updated online [31], [32]. In addition, for the sake of limited memory in practical control system, data reserving scheme is not designed in our MCFNN. Therefore, only other two strategies are considered in the proposed MCFNN structure.

1) *Data learning strategy:* During this phase, the structural adjustment and parameter updating is executed according to the following criterions.

When $\|x\| > E_a$ and $\psi < E_s$, another new membership function should be generated. Due to the fact that conventional error-based criteria are not sufficient to address the significance of input variables in the existing FNN, the spherical potential is adopted as a measure of novelty in the proposed MCFNN [33], [34]. For spherical potential, the novelty is described by the projection of the input variable x on to a hyperdimensional feature space. Due to the Gaussian function used for projection, there exists a spherical hyperdimensional feature space described by mean value and standard deviation of the Gaussian function [31]. First, define the origin of N-dimensional space as $l_0 = \frac{1}{N}\sum_{q=1}^{N} l(c_q)$. Then, the squared distance from the hyperdimensional feature centered at origin l_0 is used to express the spherical potential, which is given by

$$\psi = \|l(x) - l_0\|^2. \tag{18}$$

From [31], the expansion of the above equation can be determined as

$$\psi = l(x,x) - \frac{2}{N}\sum_{q=1}^{N} l(x, c_q) + \frac{1}{N^2}\sum_{p,q=1}^{N} l(c_p, c_q). \tag{19}$$

For Gaussian function, it is obvious that $l(x,x)$ and $\frac{1}{N^2}\sum_{p,q=1}^{N} l(c_p, c_q)$ in (19) are constants so that they can be removed from the measure of novelty. Therefore, the spherical potential ψ is defined as the following form:

$$\psi = \left| -\frac{2}{N}\sum_{q=1}^{N} l(x, c_q) \right|. \tag{20}$$

A lower potential ψ indicates that the novelty of input variable is high and a high potential indicates that the novelty is low so that no new fuzzy rules need to be added. E_s and E_a are the novelty and adding thresholds. If the value of E_a is chosen too large, few new rules will be added to capture the knowledge which will affect the generalization ability of the network. However, too low value may potentially increase the network size. As mentioned above, an input variable is novel under the circumstance that the spherical potential is close to zero. In general, E_s is chosen below 0.1 as the criteria of novelty to add a new rule. To choose the proper value of E_s and E_a, we should consider an acceptable tradeoff between network size and required accuracy.

If a new membership function is generated, the initial value of its parameters are denoted as

$$\begin{aligned} c_{N+1} &= x \\ b_{N+1} &= \kappa^* \min_{\forall j} \|x - c_q\|, q = 1, \ldots, N \\ \omega_{N+1}^o &= 0 \end{aligned} \tag{21}$$

where κ is the parameter which controls the overlap between the rule antecedents. In this article, κ is chosen in the range [0.5, 0.9]. If the value of κ is chosen too low or too larger, it will affect generalization ability, leading to adverse effects on tracking error.

Only if the following condition is met, that is, $\|x\| > E_l$, the parameters updating for membership function is triggered. In the proposed MCFNN, the parameters of membership function nearest to current input variables are adjusted according to the adaptive laws deduced from Lyapunov theorem to achieve the closed-loop stability.

Moreover, if the rule almost has no effect on the output, it will be termed as low contribution one. In this context, for purpose of reducing the computational complexity, the low contribution rule should be removed from the rule base. The contribution degree of $q\text{th}$ rule could be expressed in the following form:

$$\beta_q = l_q \max \left| x_i \omega_q^o \right|, i = 1, \ldots, n, q = 1, \ldots, N \tag{22}$$

where ω_q^o is the output weight of the $q\text{th}$ rule associated with the $o\text{th}$ output node, which is proper as a measurement of influence to the output. If $\beta_q < E_p$, the $q\text{th}$ rule should be removed. Too large E_p will lead to more rules being pruned from the network, affect the network performance diversely and even cause the closed-loop instability in practical applications. However, if $E_p$is chosen too low, fewer rules will be pruned leading to the increased network size.

2) *Data deletion strategy:* In order to avoid over-learning and sort out redundant or inefficient computation, current input variables are removed from the metacognitive component since it is not necessary to update the network parameters under the circumstance that it cannot satisfy the criterion of data learning strategy.

C. MCFNN Control Using Global Sliding Mode Control

Due to uncertain or unknown $F(X)$, the controller (9) is difficult to be realized. Considering the remarkable feature to learn any smooth functions of FNN, an MCFNN estimator can be utilized to mimic the unknown part.

Assumption 2: There exist optimal weight W^*, central vector c^*, and base width b^* to mimic uncertain term $F(X)$ which is defined as $F(X) = W^* l^* + \varepsilon$, where $l^* = l^*(X, c^*, b^*)$, ε is the mapping error. In general, ε can be assumed to be uniformly bounded as $\|\varepsilon\| \le \varepsilon_b$, where ε_b is a positive constant.

The real output of MCFNN for the estimation of uncertain part is

$$\hat{F}(X) = \hat{W}\hat{l} \in R^n \tag{23}$$

where $\hat{W} \in R^{n \times N}$ is the estimated weight vector and $\hat{l} \in R^{N \times 1}$ defined as $\hat{l} = \hat{l}(X, \hat{c}, \hat{b})$ is the estimated network parameters. It should be noted that $N_o = n$ in this context.

The optimal parameters comprise two parts using the winner rule strategy [32]. One part denotes optimal parameters of the active nearest rule, which are represented as $W^*_{\text{near}} \in R^{n \times 1}$, $b^*_{\text{near}} \in R^{n \times 1}$, and $c^*_{\text{near}} \in R^{n \times 1}$. The other part denotes inactivated rules, comprising the optimal parameters of fixed rules, which are represented as $W^*_{\text{far}} \in R^{n \times (N-1)}$, b^*_{far}, and $c^*_{\text{far}} (1 \le \text{far} \le N, \text{far} \ne \text{near})$. Hence,

$$l^*(x, c^*, b^*) = \begin{bmatrix} l^*_{\text{near}}(x, c^*_{\text{near}}, b^*_{\text{near}}) \\ l^*_{\text{far}}(x, c^*_{\text{far}}, b^*_{\text{far}}) \end{bmatrix}$$

$$W^* = \begin{bmatrix} W^*_{\text{near}} & W^*_{\text{far}} \end{bmatrix}^T.$$

Similarly, the estimates are divided into $\hat{W}_{\text{near}} \in R^{n \times 1}$, $\hat{b}_{\text{near}}$, $\hat{c}_{\text{near}} \in R^{n \times 1}$, $\hat{W}_{\text{far}} \in R^{n \times (N-1)}$, $\hat{b}_{\text{far}}$, and $\hat{c}_{\text{far}} \in R^{(N_r - n) \times 1}$.

Then, the estimated error between the real value and the output of MCFNN is defined as

$$\begin{aligned} F(X) - \hat{F}(X) &= W^*_{\text{near}} l^*_{\text{near}} - \hat{W}_{\text{near}} \hat{l}_{\text{near}} + \varepsilon \\ &= W^*_{\text{near}} (\hat{l}_{\text{near}} + \tilde{l}_{\text{near}}) - \hat{W}_{\text{near}} \hat{l}_{\text{near}} + \varepsilon \\ &= W^*_{\text{near}} \hat{l}_{\text{near}} + W^*_{\text{near}} \tilde{l}_{\text{near}} - \hat{W}_{\text{near}} \hat{l}_{\text{near}} + \varepsilon \\ &= \tilde{W}_{\text{near}} \hat{l}_{\text{near}} + \hat{W}_{\text{near}} \tilde{l}_{\text{near}} + \varepsilon_0 \end{aligned} \tag{24}$$

where $\varepsilon_0 = \tilde{W}_{\text{near}} \tilde{l}_{\text{near}} + \varepsilon$.

The linearization theorem of Taylor expansion is utilized to represent the uncertain function by a partially linear one and the expansion of $\tilde{l}$ is denoted in the following form:

$$\begin{aligned} \tilde{l}_{\text{near}} &= \frac{\partial l_{\text{near}}}{\partial c_{\text{near}}} \Big|_{c=\hat{c}} (c^*_{\text{near}} - \hat{c}_{\text{near}}) \\ &\quad + \frac{\partial l_{\text{near}}}{\partial b_{\text{near}}} \Big|_{b=\hat{b}} (b^*_{\text{near}} - \hat{b}_{\text{near}}) + O_h \\ &= l_c \cdot \tilde{c}_{\text{near}} + l_b \cdot \tilde{b}_{\text{near}} + O_h \end{aligned} \tag{25}$$

where $\tilde{c}_{\text{near}}, \tilde{b}_{\text{near}}$ are represented as following:

$$\begin{aligned} \tilde{c}_{\text{near}} &= c^*_{\text{near}} - \hat{c}_{\text{near}} \in R^{n \times 1} \\ \tilde{b}_{\text{near}} &= b^*_{\text{near}} - \hat{b}_{\text{near}} \in R^{n \times 1}. \end{aligned} \tag{26}$$

l_c, l_b in (25) can be determined as

$$l_c = \left[\frac{\partial l_{\text{near}}}{\partial c_1^{\text{near}}} \cdots \frac{\partial l_{\text{near}}}{\partial c_i^{\text{near}}} \cdots \frac{\partial l_{\text{near}}}{\partial c_n^{\text{near}}} \right] \Big|_{c==\hat{c}} \in R^{1 \times n} \tag{27}$$

$$l_b = \left[\frac{\partial l_{\text{near}}}{\partial b_1^{\text{near}}} \cdots \frac{\partial l_{\text{near}}}{\partial b_i^{\text{near}}} \cdots \frac{\partial l_{\text{near}}}{\partial b_n^{\text{near}}} \right] \Big|_{b==\hat{b}} \in R^{1 \times n}. \tag{28}$$

For the stability of the system, the control law is designed as

$$U = \frac{B^{-1}}{C} [\dot{g}(t) - C\hat{F}(X) + C\dot{X}_d - D\text{sgn}(S)]. \tag{29}$$

Theorem 1: Consider a class of universal dynamic systems with parameter perturbation and external disturbance represented by (3), if the MCFNN law is formulated as (29), the corresponding adaptation laws for MCFNN parameters are designed as (30)–(32), then the asymptotic stability of the proposed MCFNN system can be guaranteed. The block diagram of the controller is shown in Fig. 2

$$\dot{\hat{W}}^T_{\text{near}} = -\eta_1 S^T C \hat{l}_{\text{near}} \tag{30}$$

$$\dot{\hat{c}}^T_{\text{near}} = -\eta_2 S^T C \hat{W}_{\text{near}} l_c \tag{31}$$

$$\dot{\hat{b}}^T_{\text{near}} = -\eta_3 S^T C \hat{W}_{\text{near}} l_b \tag{32}$$

where η_1, η_2, and η_3 are positive learning rates.

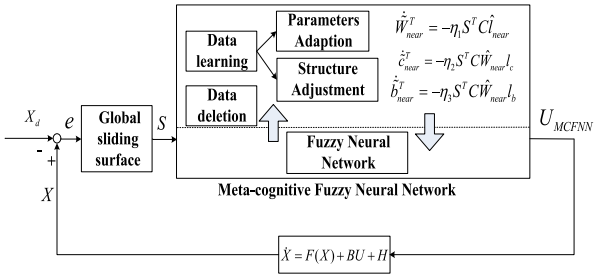

Fig. 2. Block diagram of metacognitive fuzzy-neural-network control using global sliding mode control.

Proof: The following Lyapunov function candidate is defined as

$$V_2 = \frac{1}{2}S^T S + \frac{1}{2\eta_1}tr(\tilde{W}_{\text{near}}^T \tilde{W}_{\text{near}}) + \frac{1}{2\eta_2}tr(\tilde{c}_{\text{near}}^T \tilde{c}_{\text{near}}) + \frac{1}{2\eta_3}tr(\tilde{b}_{\text{near}}^T \tilde{b}_{\text{near}}) \tag{33}$$

$\frac{1}{2\eta_1}tr(\tilde{W}_{\text{near}}^T \tilde{W}_{\text{near}}) + \frac{1}{2\eta_2}tr(\tilde{c}_{\text{near}}^T \tilde{c}_{\text{near}}) + \frac{1}{2\eta_3}tr(\tilde{b}_{\text{near}}^T \tilde{b}_{\text{near}})$ is denoted as M for the sake of illustration.

Deriving V_2 with respect to time and substituting the controller (29) into it, the following expression can be obtained:

$$\dot{V}_2 = S^T \dot{S} + \dot{M} = S^T[C(\tilde{W}_{\text{near}} \hat{l}_{\text{near}} + \hat{W}_{\text{near}} \tilde{l}_{\text{near}} + \varepsilon_0) + \text{CH} - D\text{sgn}(S)] + \dot{M}. \tag{34}$$

Then, substituting the Taylor expansion into (34), it can be obtained that

$$\begin{aligned}\dot{V}_2 = {} & S^T C\tilde{W}_{\text{near}} \hat{l}_{\text{near}} + S^T C\hat{W}_{\text{near}}(l_c \cdot \tilde{c}_{\text{near}} + l_b \cdot \tilde{b}_{\text{near}}) \\ & + S^T CO_{ho} + S^T CH - S^T D\text{sgn}(S) \\ & + \frac{1}{\eta_1}tr(\dot{\tilde{W}}_{\text{near}}^T \tilde{W}_{\text{near}}) \\ & + \frac{1}{\eta_2}tr(\dot{\tilde{c}}_{\text{near}}^T \tilde{c}_{\text{near}}) + \frac{1}{\eta_3}tr(\dot{\tilde{b}}_{\text{near}}^T \tilde{b}_{\text{near}})\end{aligned} \tag{35}$$

where $O_{ho} = \varepsilon_0 + \hat{W}_{\text{near}} O_h$.

Using (30)–(32), (35) can be rewritten as

$$\begin{aligned}\dot{V}_2 &= S^T[CH + CO_{ho}] - S^T D\text{sgn}(S) \\ &= S^T(CH + CO_{ho}) - D\|S\| \\ &\le \|S\|(CH_M + CO_M - D).\end{aligned} \tag{36}$$

O_{ho} is assumed to be uniformly bounded as $\|O_{ho}\| \le O_M$. The following inequality can be obtained if $D > C(H_M + O_M)$.

$$\dot{V}_2 < 0. \tag{37}$$

The negative definite of $\dot{V}_2$ suggests that V_2, S both are bounded. It can be concluded that $\dot{S}$ is bounded. The inequality $\dot{V}_2 \le \|S\|(CH_M + CO_M - D)$ indicates that S is integrable as $\int_0^t \|S\|dt \le \frac{1}{CH_M + CO_M - D}[V(t) - V(0)]$. It can be obtained that $\lim_{t\to\infty} \int_0^t \|S\|\, dt$ is bounded since $V(0)$ is bounded and $V(t)$ is bounded and nonincreasing. Since $\lim_{t\to\infty} \int_0^t \|S\|\, dt$ and $\dot{S}$ are bounded, according to Barbalat's lemma, $S(t)$ will achieve $\lim_{t\to\infty} S(t) = 0$. Therefore, the control force can assure the asymptotical stability of closed-loop system and high accuracy tracking performance. One can conclude that GSMC using MCFNN can achieve global robust and low computational burden even with uncertain or unknown functions.

IV. Simulation and Experimental Validation for Active Power Filter

In this section, the performance of proposed SOGSMC is illustrated by two examples, which is described next.

Example 1: In this example, the performance of proposed control approach is studied through an APF [23]. The APF model is described as following:

$$\dot{X} = F(X) + BU + H \tag{38}$$

where $X = [i_1 i_2 i_3]^T$, $F(X) = [-\frac{R_{c1}}{L_{c1}} i_1 + \frac{v_1}{L_{c1}} - \frac{R_{c1}}{L_{c1}} i_2 + \frac{v_2}{L_{c1}} - \frac{R_{c1}}{L_{c1}} i_3 + \frac{v_3}{L_{c1}}]^T$, $B = -\frac{V_{\text{dc}}}{L_{c1}}$, $U = [\,u_1\ u_2\ u_3\,]^T$, and H is lumped uncertainties.

To achieve the target of purifying harmonics, APF usually requires multiple sensors to detect load current, compensation current (system state in the proposed control system), grid-side voltage, and dc-link voltage. It can be seen from (38) that there exist v_1, v_2, and v_3 in $F(X)$. In practical operation, once the grid-side voltage sensor fails, incorrect v_1, v_2, and v_3 leading to incorrect $F(X)$ will significantly affect the control performance in reality, and even lead the system to instability. Therefore, it is essential that $F(X)$ is termed as an unknown or uncertain part of APF due to sensor fault of grid-side voltage, and it should be well estimated by MCFNN approximator. In addition, fault detection and fault-tolerant control schemes in [15], [35] also are effective for measurement noise and sensor fault, which will be further studied in our further work.

In practical operation, APF is equivalent to a flow control current source which contains three sections, reference generation module, control system, and main circuit. It is worth noticing that the performance of an APF depends not only on the reference tracking performance, but also the accuracy of the reference generation. The $i_p - i_q$ algorithm is utilized as harmonic current detection method in reference generation module, where the reference currents should be the same magnitudes and opposite phases with the harmonic currents [36], [37]. The block diagram for $i_p - i_q$ algorithm is shown in Fig. 3, where i_1, i_2, and i_3 are detected load currents, i_{1f}, i_{2f}, and i_{3f} are fundamental currents, i_1^*, i_2^*, i_3^* are harmonic currents. i_p and i_q are active current and reactive current, respectively, i_{p1} and i_{q1} are fundamental active current and fundamental reactive current, respectively, and V_s is source voltage. Their mathematical relationship is

$$\begin{bmatrix} i_p \\ i_q \end{bmatrix} = CC_{32} \begin{bmatrix} i_1 \\ i_2 \\ i_3 \end{bmatrix} \tag{39}$$

$$C_{32} = \sqrt{\frac{2}{3}} \begin{bmatrix} 1 & -1/2 & -1/2 \\ 0 & \sqrt{3}/2 & -\sqrt{3}/2 \end{bmatrix} \tag{40}$$

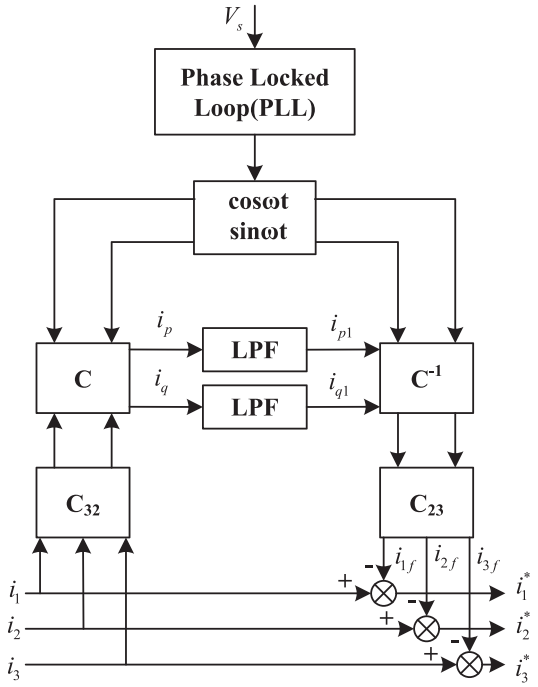

Fig. 3. Block diagram for reference generation.

$$C = \begin{bmatrix} \sin\omega t & -\cos\omega t \\ -\cos\omega t & -\sin\omega t \end{bmatrix} \tag{41}$$

$$\begin{bmatrix} i_{1f} \\ i_{2f} \\ i_{3f} \end{bmatrix} = C_{23}C^{-1} \begin{bmatrix} i_{p1} \\ i_{q1} \end{bmatrix} \tag{42}$$

$$\begin{bmatrix} i_1^* \\ i_2^* \\ i_3^* \end{bmatrix} = \begin{bmatrix} i_1 \\ i_2 \\ i_3 \end{bmatrix} - \begin{bmatrix} i_{1f} \\ i_{2f} \\ i_{3f} \end{bmatrix}. \tag{43}$$

The aim of this control problem is to use proposed control strategy to make the compensation current i_c track reference current i_{cref}.

In the MCFNN, the initial values of the central vector are set as $c = [-2\ -1\ 0\ 1\ 2]^T$, the initial values of base width are set as $b = [1\ 1\ 1\ 1\ 1]^T$, and the initial weights are chosen as random numbers between -1 and 1. $E_a = 5$, $E_s = 0.02$, $\kappa = 0.8$, $E_p = 0.2$, $C = 1000$, $\eta_1 = 1, \eta_2 = 0.01, \eta_3 = 0.01$, $D = 1000$, and $k = 100$. Table I shows the system parameters for example 1.

Load current is illustrated in Fig. 4(a). Also, harmonic spectrum of the load current is shown in Fig. 4(b). It is seen that there are abundant harmonics in load current and the total harmonic distortion (THD) is up to 24.72%. Source current is shown in Fig. 5. As it can be seen, using APF with the proposed controller, the source current is close to sinusoidal with its THD reduced to 1.70% which demonstrates that the source current is purified efficiently.

The simulation results under load variations are presented in Figs. 6 and 7. This figure shows, from top to bottom, source voltage, load current, source current, compensation current, reference current, tracking error, and dc voltage. It can be noted that the output compensation current of APF can be modified quickly to eliminate the harmonics effectively and dc voltage is forced to a stable state during a change in the load current. In MCFNN, fuzzy rules can be generated or pruned at certain instant. So, the rule base has a clear learning process and arrives at a stable state with three rules in Fig. 7. It is noteworthy that there are five fuzzy rules in FNN during a trial-and-error process in [23] which imposes more computational burden. Thus, one

TABLE I
SYSTEM PARAMETERS

Supply voltage and frequency	$V_{s1} = V_{s2} = V_{s3} = 220$ V, $f = 50$ Hz
Nonlinear load	$R = 5\ \Omega$, $L = 10$ mH
Active power filter parameters	$L_c = 10$ mH, $R_c = 0.1\ \Omega$, $C = 2200$ mH, $v_{dcref} = 1000$ V
Switching frequency	$f_{sw} = 10$ kHz

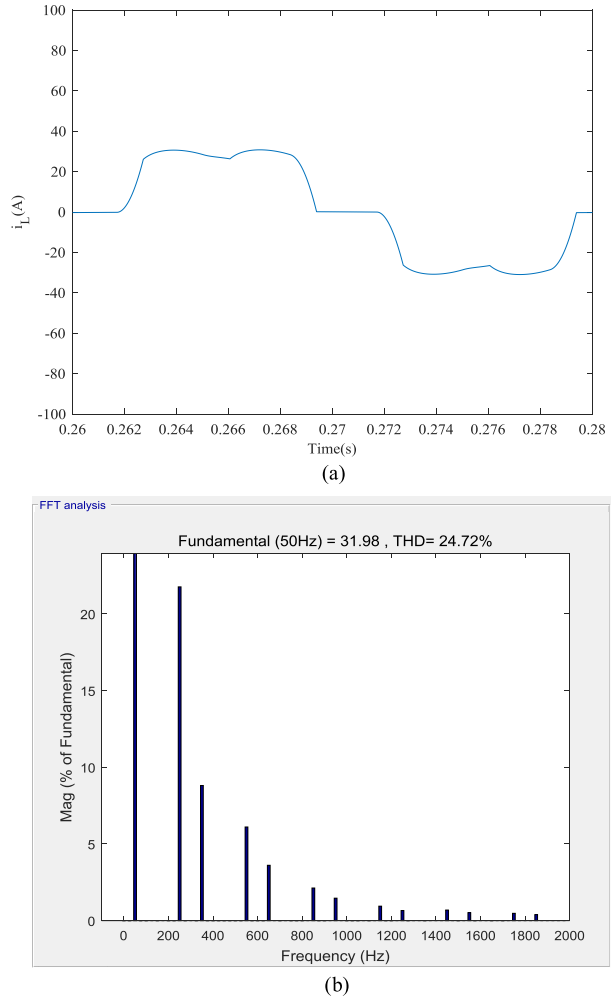

Fig. 4. (a) Load current. (b) Harmonic spectrum of load current.

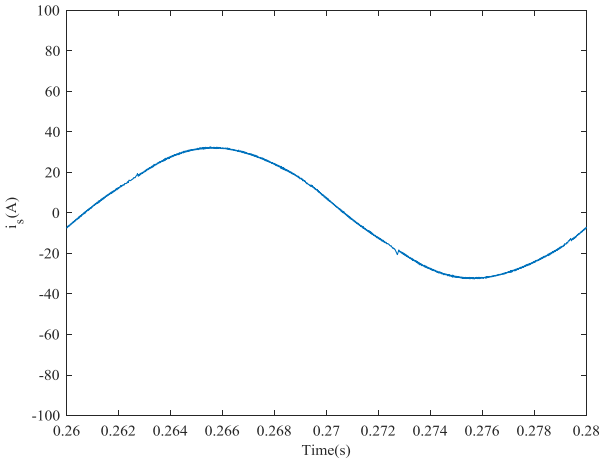

(a)

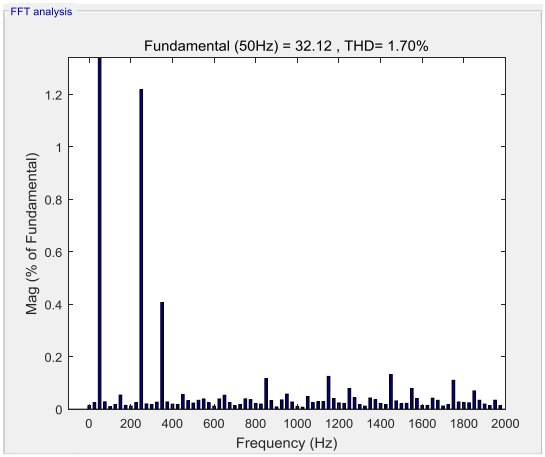

(b)

Fig. 5. (a) Source current after harmonics compensation. (b) Harmonic spectrum of source current after harmonics compensation.

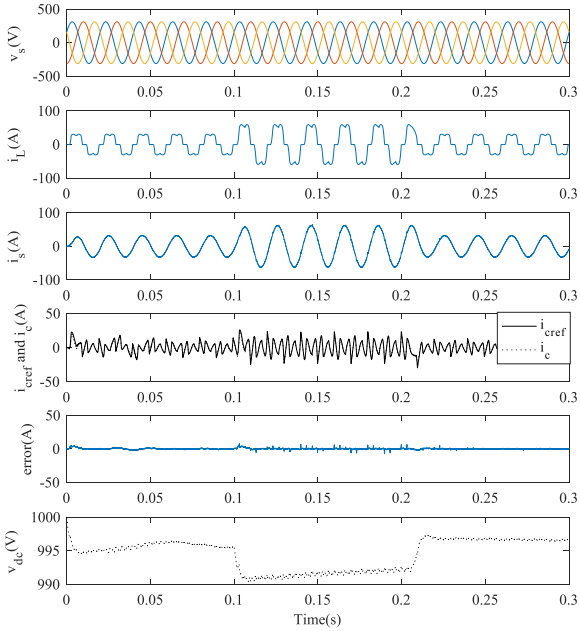

Fig. 6. Simulation results of APF under load variations.

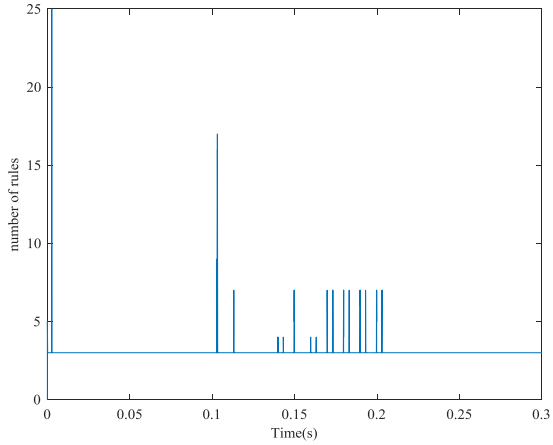

Fig. 7. Rule evolvement.

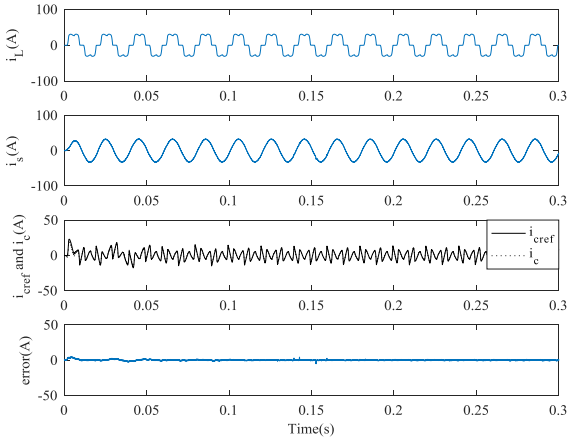

Fig. 8. Simulation results of APF with the variation in inductance.

can obtain that APF with SOGSMC reveal remarkable features in dynamic and static.

In order to verify the transient performance of the controller in case of dynamic parameter variation, ac inductance varies from 10 to 12 mH at $t = 0.1$ s and from 12 to 10 mH at $t = 0.2$ s in Fig. 8, and dc capacitance varies from 2200 to 1100 μF at $t = 0.1$ s and from 1100 to 2200 μF at $t = 0.2$ s in Fig. 9, respectively. It is noteworthy that the source current is still close to sinusoidal with parameters perturbation, and remarkable transient performance of the proposed control can be confirmed from Figs. 8 and 9.

To further test the outstanding property of the proposed SOGSMC, we also give simulation results with other advanced control schemes, such as adaptive fuzzy sliding control (AFSC) [38] and adaptive fuzzy backstepping control (AFBC) [39]. When comparing performance of the three control methods in simulations and experiments, we use the identical reference generation method based on $i_p - i_q$. Note that AFSC and AFBC in [38], [39] both are designed for APF and proved to be effective so that the comparative simulation results are convincing. The following root-mean-square-error (RMSE) is taken as the

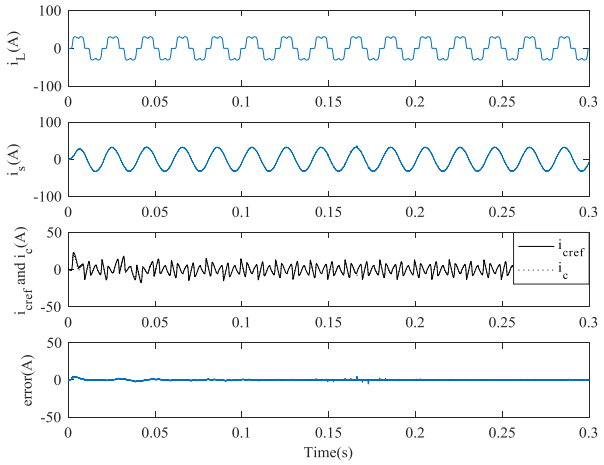

Fig. 9. Simulation results of APF with the variation in dc capacitance.

TABLE II
COMPARISONS OF ROOT MEAN SQUARE ERRORS

Methods	AFSC	AFBC	MCFNN
RMSE	0.5798	0.9525	0.3620

TABLE III
SYSTEM PARAMETERS AND COMPONENTS FOR EXPERIMENT

Supply voltage and frequency	$V_s = 24$ V, $f = 50$ Hz
Nonlinear load	$R = 15\ \Omega$, $C = 1$ mF
Active power filter parameters	$L_c = 10$ mH, $R_c = 0.1\ \Omega$, $C = 2200\ \mu$F, $v_{dcref} = 50$ V
Switching frequency	$f_{sw} = 20$ kHz
AC source	IT7324, ITECH
Power IGBTs	SKM75GB12T4, SEMIKON
IGBT drivers	SKYPER_32_R, SEMIKON
Voltage sensors	CHV-25P, Beijing SENSOR
Current sensors	CSM003A, CHIEFUL
Auxiliary power supply	DP831, RIGOL

current tracking performance measure to do the comparison.

$$\mathrm{RMSE} = \sqrt{\frac{1}{T}\sum_{d=1}^{T} e^2(d)}$$

where T is the total number of tracking error. According to the RMSE measures in Table II, proposed SOGSMC has over 38% and 62% tracking improvement than AFSC and AFBC, respectively. From this, we can conclude that tracking performance of SOGSMC is better than AFSC and AFBC.

Example 2: In this example, the proposed control approach is further evaluated with the experimental results of APF in Figs. 10–18. Nominal values of system parameters and components are collected in Table III.

The steady-state experimental results are presented in Figs. 11 and 12. Fig. 11 presents the steady-state experimental results of source voltage, load current, compensation current supplied by APF, and source current. There are abundant harmonics in load current and the THD is up to 30.28%. As it can be seen, using APF with the proposed controller, the source current is close to

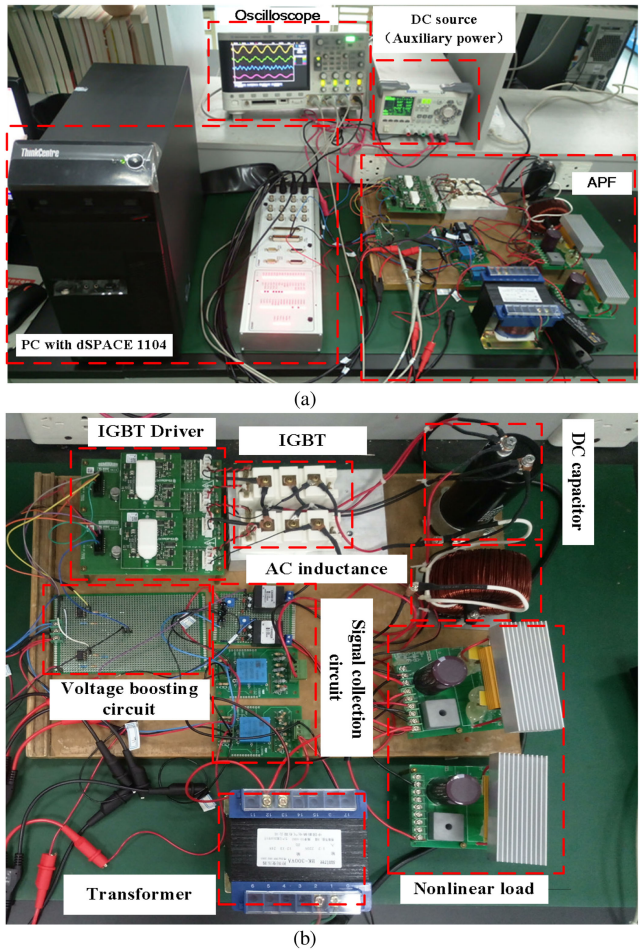

Fig. 10. Experimental prototype developed in the laboratory. (a) Overall structure. (b) APF.

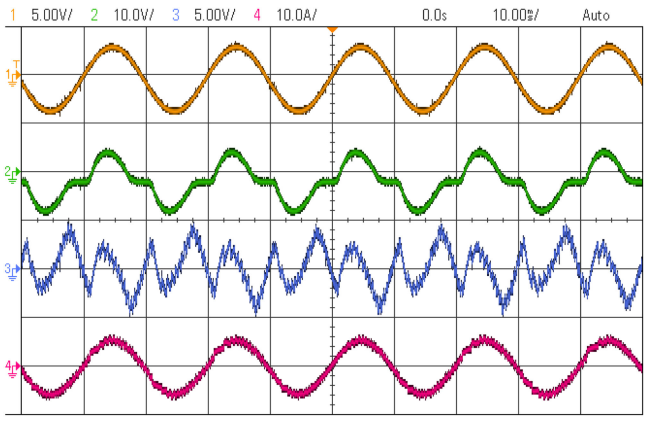

Fig. 11. Steady-state experimental results.

sinusoidal with its THD reduced to 3.26% which demonstrates that the source current is purified efficiently.

Fig. 13 presents the dynamic experimental results. It can be noted that the output compensation current of APF can be modified quickly to eliminate the harmonics effectively during a change in the load current. Thus, one can obtain that APF with SOGSMC reveal remarkable features in dynamic and static.

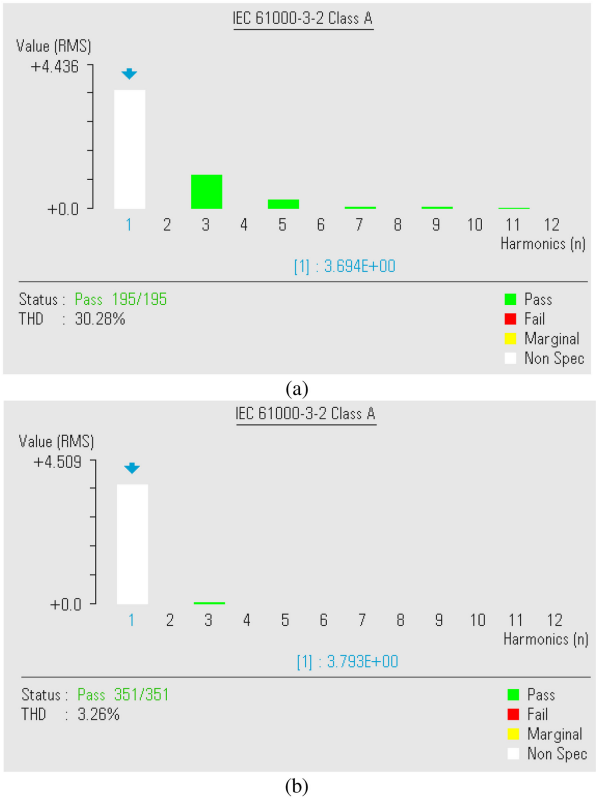

Fig. 12. Harmonic spectrum of source current. (a) Without APF. (b) With APF.

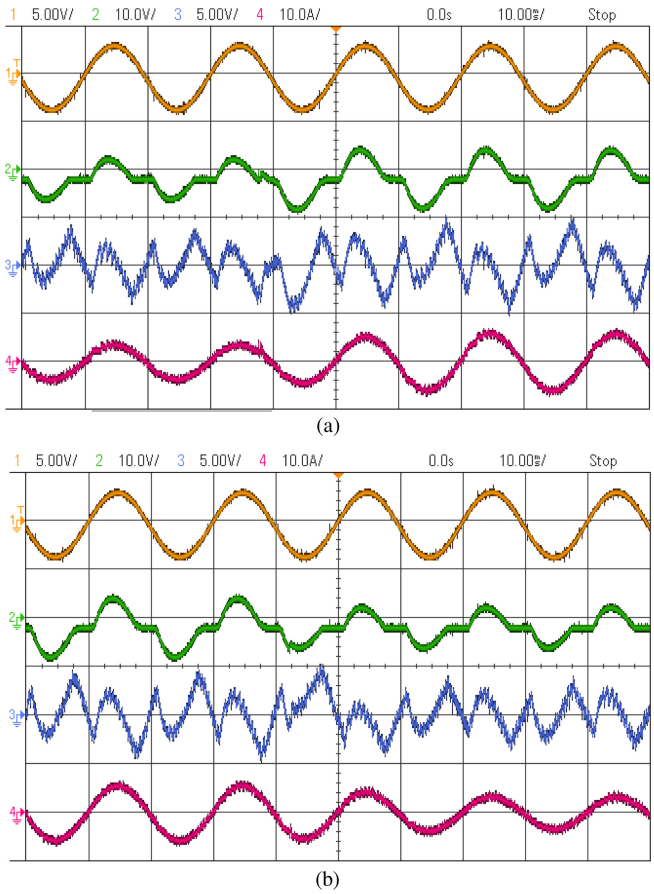

Fig. 13. Dynamic experimental results. (a) Loads increase. (b) Loads decrease.

In order to demonstrate the superiority of SOGSMC in strong robustness with parameter uncertainties, an APF with the parameter uncertainties is executed. As shown in Figs. 14–16, it is noted that the source current is still close to sinusoidal with parameters variation in the inductance and the dc capacitance which can represent the parametric perturbation. It can be concluded that SOGSMC has good robustness to the parameter variations.

To further test the remarkable feature of SOGSMC, experimental results using other advanced control strategies for APF, such as AFSC [38] and AFBC [39], are shown in Figs. 17 and 18. It is noteworthy that different control methods lead to similar harmonic suppression performance in Figs. 17 and 18. However, the THD of the proposed SOGSMC is smaller than that of its competitors, more than 15% and 37%, respectively. Taking into consideration structure-adjustment and parameter-adaptive capability, the proposed SOGSMC shows superior performance for APF compared with other existing advanced control schemes.

Remark 3: For APF, H in the mathematical expression (38) represents the main characteristics of the lumped uncertainties. It is an integration of unknown equivalent resistance and other perturbed components containing reactors and power capacitors, and the uncertain external disturbances including the load perturbations. The lumped uncertainties can be assumed to be bounded in practical systems. However, as the value of D lies on the supremum of lumped uncertainties, the problem is their supremum, which is not easy to measure accurately, resulting in the difficulty in realizing the controller. In the ordinary GSMC, D should be larger than their supremum, which always leads to chattering phenomenon. Whereas, due to the use of saturation function, the chattering phenomenon will be further alleviated, which is highly preferable in APF.

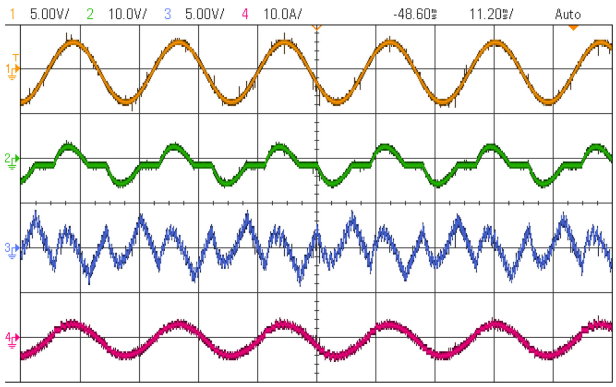

Fig. 14. Experimental results with $L_c = 10$ mH, $C = 1100$ μF.

Remark 4: In the ordinary SMC, due to the fact that the sliding regime may occur only near the origin of phase plane and the response during the reaching phase is sensitive to system perturbation, robust performance is not ensured [40]. For the proposed GSMC scheme, the sliding surface is designed such that the initial state is located on it; then the system states are constrained to the sliding regime by an SMC. Therefore, the sliding mode invariably exists and robust performance is ensured

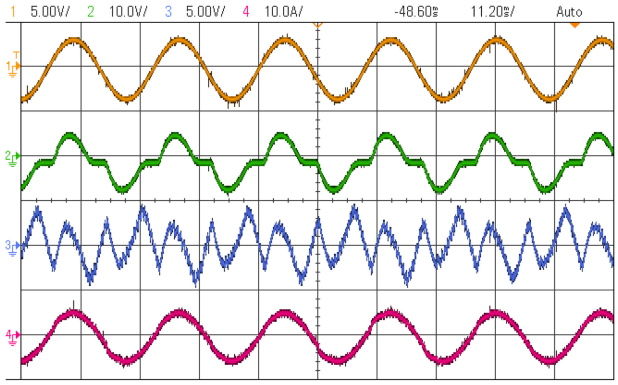

Fig. 15. Experimental results with $L_c = 12$ mH, $C = 1100$ μF.

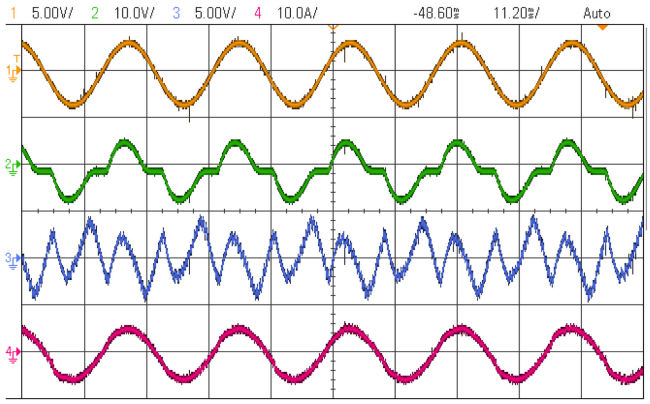

Fig. 16. Experimental results with $L_c = 12$ mH, $C = 2200$ μF.

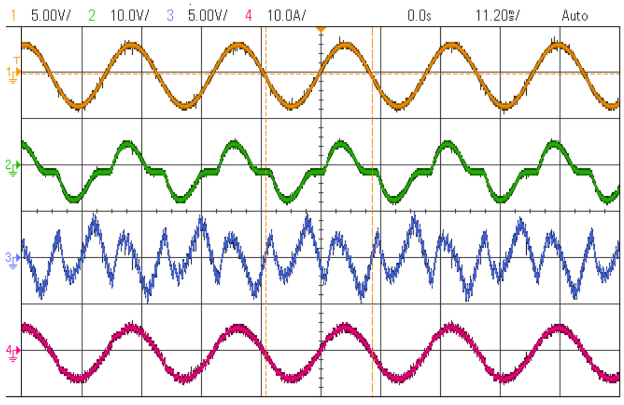

(a)

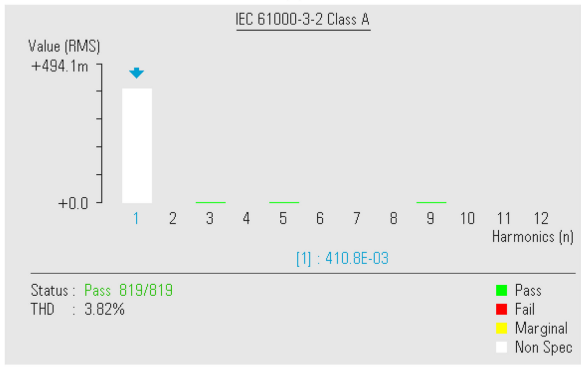

(b)

Fig. 17. Experimental results using AFSC. (a) Experimental waveforms. (b) Harmonic spectrum of source current.

throughout an entire response. There are three conditions for $g(t)$ in the proposed sliding surface. Condition (1) implies that the system state is initially located in the sliding regime. Condition (2) implies the asymptotic stability of the closed-loop system. Condition (3) is required for the existence of a sliding mode. If Conditions (1)–(3) are satisfied and the control law is designed such that the sliding condition holds near the sliding regime, asymptotic stability is ensured and the sliding mode exists continually so that robustness is ensured throughout the entire response.

Remark 5: As can be seen from (3), B considered in this article is a constant matrix with no uncertainties. Although the assumption of B is a strong restriction, many physical systems, such as automobile electronic throttle [13], surface vehicles [24], hybrid maglev transportation system [41], can be described in the form of system (3). In [13], [24], [41], we can see that the coefficients of control inputs are constants. Without loss of generality, a class of uncertain dynamic systems is considered in the future work, whose form is given as $\dot{X} = F(X) + G(X)U + H$, where $F(X)$ and $G(X)$ are assumed to be unknown and bounded nonlinear functions. To handle $F(X)$ and $G(X)$, we can utilize two MCFNNs to estimate them. It is worth noticing that the output weight and parameter updating laws for the estimation of $G(X)$ using MCFNN will be different from that used for estimating $F(X)$. Based on the contribution of this article, we can carry out the similar design process to redesign the output weight and parameter updating laws for the estimation of $G(X)$ in the universal dynamic systems (2). However, it will increase the computation burden due to so many adaptive laws. In [35], [42], [43], other effective schemes for handling $G(X)$ in nonlinear system are developed, where $G(X)$ can be coped with a simpler form in the controllers. The detailed explorations for universal dynamic systems can be developed in our future work.

Remark 6: APF discussed in this study can be described by system (3). The operation of APF can be controlled using outer voltage loop and inner current loop. The main control objective of outer voltage loop is to regulate the dc-link capacitor voltage. In this article, PI regulator is adopted to minimize the error between actual $V_{\rm dc}$ and reference dc-link voltage. The main aim of inner current loop is to track the reference signals, which is the key to achieve the target of purifying harmonics. It is worth noting that $V_{\rm dc}$ can be regulated at an expected value with PI control and the change of dc-side voltage is far less than that of compensation current. So, dc-side voltage can be treated as a constant in the design of inner current loop (the proposed MCFNN control). L_{c1} is the nominal value of inductor, which also can be termed as a constant. Thus, $B = -\frac{V_{\rm dc}}{L_{c1}}$ is classified as a constant term with no need to estimate. So we use MCFNN to estimate $F(X)$ instead of $F(X)$ and B. Moreover, simulation and experimental results demonstrate that the proposed MCFNN control is effective to achieve the control aim for APF.

Remark 7: To further simplify the tuning procedure of prespecified parameters for practical implementation, the

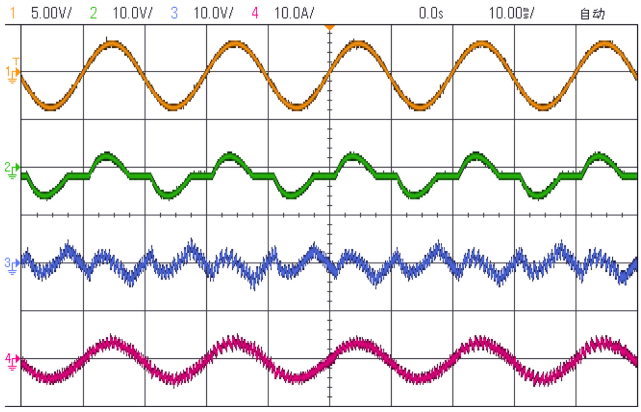

(a)

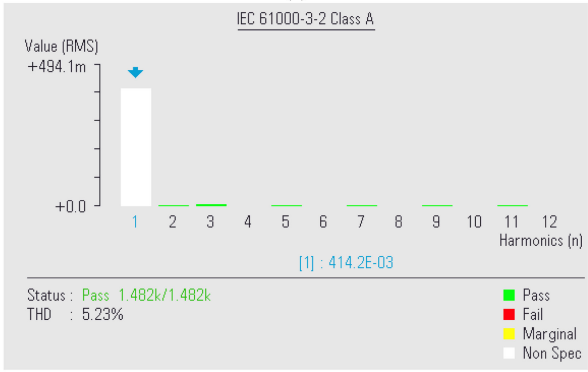

(b)

Fig. 18. Experimental results using AFBC. (a) Experimental waveforms. (b) Harmonic spectrum of source current.

detailed parameter selection criteria are summarized as follows. Considering the GSMC parameter values of C and k, these parameters are determined by trial and error with some empirical rules. C and k can influence the convergence rate and the tracking performance. The larger values of C and k, the faster error convergence rate, but their values should be limited in practical implementation due to control saturation. The choice of the value of D has a significant effect on the control performance. If D is chosen too large, the sign function will cause the undesired chattering phenomena. However, the control system may be unstable if D is chosen too small. Moreover, the parameters η_1, η_2, and η_3 should be positive constants based on Lyapunov theorem. By empirical rules, larger values of η_1, η_2, and η_3 could result in divergence control responses. On the other hand, smaller values of η_1, η_2, and η_3 could result in slow convergence of the control performance. It is worth noticing that η_1 is always larger than η_2 and η_3 since the weight vector matrix dominates the major network output. In addition, when determining the values of E_a, E_s, κ, and E_p, we need to consider an acceptable tradeoff between control performance and computational burden. For example, smaller value of E_p can remove more rules and reduce computation burden with the sacrifice of the degraded control performance due to the lower learning capability.

Remark 8: It is worth noting that unlike Quasi-GSMC in this article, high-order SMC is also an effective scheme to deal with chattering phenomenon [44]. Different from conventional first-order SMC, the construction of the control law in high-order SMC is formularized using the derivative of sliding mode function, leading into continuous control law and alleviating the chattering problem in theory. Thus, some explorations using high-order SMC for APF can be developed in the immediate future.

Remark 9: In recent years, the remarkable development of very large-scale integration has boosted the improvement of computing power of microprocessors unprecedentedly. In this context, intelligent control strategies with computational complexity could be achieved using a high-performance microprocessor. Thus, it is not difficult to achieve the proposed SOGSMC via current dSPACE or DSP with high performance cores. In addition, detailed experimental results in Figs. 11–18 have revealed the superior values of the proposed GSMC using MCFNN for practicing engineers.

V. Conclusion

An SOGSMC is developed in this study to achieve superior tracking property of multiinput universal dynamic systems with uncertainties. In addition to the remarkable characteristics of global robustness and chattering free, the structure of the proposed MCFNN can be updated online and zero convergence ability also can be ensured with rigorous stability analysis deduced from Lyapunov theorem. In the rule evolvement, the membership functions are dynamically adjusted and pruned so that the proposed SOGSMC can acquire unexpected dynamic changes. The simulation and experimental validations for APF verify that the proposed schemes can realize better control performance with less fuzzy rules than traditional FNN, showing high harmonic elimination ability under various conditions.

Acknowledgment

The authors would like to express their sincere thanks to the editors and all the reviewers for the constructive suggestions that have greatly improved the quality of this article.

References

[1] N. Sun, D. Liang, Y. Wu, Y. Chen, Y. Qin, and Y. Fang, "Adaptive control for pneumatic artificial muscle systems with parametric uncertainties and unidirectional input constraints," *IEEE Trans. Ind. Informat.*, to be published, doi: 10.1109/TII.2019.2923715.

[2] M. Hua, D. Zheng, F. Deng, J. Fei, P. Cheng, and X. Dai, "H∞ filtering for nonhomogeneous Markovian jump repeated scalar nonlinear systems with multiplicative noises and partially mode-dependent characterization," *IEEE Trans. Syst., Man, Cybern., Syst.*, to be published, doi: 10.1109/TSMC.2019.2919146.

[3] H. Li, P. Shi, and D. Yao, "Adaptive sliding-mode control of Markov jump nonlinear systems with actuator faults," *IEEE Trans. Autom. Control*, vol. 62, no. 4, pp. 1933–1939, Apr. 2017.

[4] H. Pan and W. Sun, "Nonlinear output feedback finite-time control for vehicle active suspension systems," *IEEE Trans. Ind. Informat.*, vol. 15, no. 4, pp. 2073–2082, Apr. 2019.

[5] G. P. Incremona, M. Rubagotti, and A. Ferrara, "Sliding mode control of constrained nonlinear systems," *IEEE Trans. Autom. Control*, vol. 62, no. 6, pp. 2965–2972, Jun. 2017.

[6] W. Liu, G. Xu, and X. Jiang, "Discrete global sliding mode control for time-delay carbon fiber multilayer diagonal loom," *IEEE Access*, vol. 5, pp. 15326–15331, 2017.

[7] Y. Chu, J. Fei, and S. Hou, "Dynamic global proportional integral derivative sliding mode control using radial basis function neural compensator for three-phase active power filter," *Trans. Inst. Meas. Control*, vol. 40, no. 12, pp. 3549–3559, 2018.

[8] D. Efimov and L. Fridman, "Global sliding-mode observer with adjusted gains for locally Lipschitz systems," *Automatica*, vol. 47, no. 3, pp. 565–570, 2011.
[9] Z. Hu *et al.*, "Global sliding mode control based on a hyperbolic tangent function for matrix rectifier," *J. Power Electron.*, vol. 17, no. 4, pp. 991–1003, 2017.
[10] S. Mobayen and D. Baleanu, "Linear matrix inequalities design approach for robust stabilization of uncertain nonlinear systems with perturbation based on optimally-tuned global sliding mode control," *J. Vib. Control*, vol. 23, no. 8, pp. 1285–1295, May 2017.
[11] M. L. Nguyen, X. K. Chen, and F. Yang, "Discrete-time quasi-sliding-mode control with prescribed performance function and its application to piezo-actuated positioning systems," *IEEE Trans. Ind. Electron.*, vol. 65, no. 1, pp. 942–950, Jan. 2017.
[12] D. Simon, *Optimal State Estimation*. Hoboken, NJ, USA: Wiley, 2006.
[13] H. Wang *et al.*, "Adaptive integral terminal sliding mode control for automobile electronic throttle via an uncertainty observer and experimental validation," *IEEE Trans. Veh. Technol.*, vol. 67, no. 9, pp. 8129–8143, Sep. 2018.
[14] P. Shi, Y. Xia, G. P. Liu, and D. Rees, "On designing of sliding-mode control for stochastic jump systems," *IEEE Trans. Autom. Control*, vol. 51, no. 1, pp. 97–103, Jan. 2006.
[15] P. Shi, M. Liu, and L. Zhang, "Fault-tolerant sliding-mode-observer synthesis of Markovian jump systems using quantized measurements," *IEEE Trans. Ind. Electron.*, vol. 62, no. 9, pp. 5910–5918, Sep. 2015.
[16] Y. Chu, J. Fei, and S. Hou, "Adaptive global sliding-mode control for dynamic systems using double hidden layer recurrent neural network structure," *IEEE Trans. Neural Netw. Learn. Syst.*, to be published, doi: 10.1109/TNNLS.2019.2919676.
[17] J. Fei and Y. Chu, "Double hidden layer output feedback neural adaptive global sliding mode control of active power filter," *IEEE Trans. Power Electron.*, presto be published, doi: 10.1109/TPEL.2019.2925154.
[18] T. Yang, N. Sun, H. Chen, and Y. Fang, "Neural network-based adaptive antiswing control of an underactuated ship-mounted crane with roll motions and input dead zones," *IEEE Trans. Neural Netw. Learn. Syst.*, to be published, doi: 10.1109/TNNLS.2019.2910580.
[19] X. Su, F. Xia, J. Liu, and L. Wu, "Event-triggered fuzzy control of nonlinear systems with its application to inverted pendulum systems," *Automatica*, vol. 94, pp. 236–248, 2018.
[20] X. Cao, P. Shi, Z. Li, and M. Liu, "Neural-network-based adaptive backstepping control with application to spacecraft attitude regulation," *IEEE Trans. Neural Netw. Learn. Syst.*, vol. 29, no. 9, pp. 4303–4313, Sep. 2018.
[21] C. Sun, H. Gao, W. He, and Y. Yu, "Fuzzy neural network control of a flexible robotic manipulator using assumed mode method," *IEEE Trans. Neural Netw. Learn. Syst.*, vol. 29, no. 11, pp. 5214–5227, Nov. 2018.
[22] P. Shi, Y. Zhang, M. Chadli, and R. K. Agarwal, "Mixed H-infinity and passive filtering for discrete fuzzy neural networks with stochastic jumps and time delays," *IEEE Trans. Neural Netw. Learn. Syst.*, vol. 27, no. 4, pp. 903–909, Apr. 2016.
[23] S. Hou, J. Fei, C. Chen, and Y. Chu, "Finite-time adaptive fuzzy-neural-network control of active power filter," *IEEE Trans. Power Electron.* vol. 34, no. 10, pp. 10298–10313, Oct. 2019.
[24] N. Wang and M. Joo Er, "Self-constructing adaptive robust fuzzy neural tracking control of surface vehicles with uncertainties and unknown disturbances," *IEEE Trans. Control Syst. Technol.*, vol. 23, no. 3, pp. 991–1002, May 2015.
[25] L. Wu and M. Wu, "Single-phase cascaded H-bridge multi-level active power filter based on direct current control in AC electric railway application," *IET Power Electron.*, vol. 10, no. 6, pp. 637–645, 2017.
[26] N. G. M. Thao, K. Uchida, K. Kofuji, T. Jintsugawa, and C. Nakazawa, "An automatic-tuning scheme based on fuzzy logic for active power filter in wind farms," *IEEE Trans. Control Syst. Technol.*, vol. 27, no. 4, pp. 1694–1702, Jul. 2019.
[27] F. Lin, S. Chen, and C. Hsu, "Intelligent backstepping control using recurrent feature selection fuzzy neural network for synchronous reluctance motor position servo drive system," *IEEE Trans. Fuzzy Syst.*, vol. 27, no. 3, pp. 413–427, Mar. 2019.
[28] H. Han, X. Wu, and J. Qiao, "A self-organizing sliding-mode controller for wastewater treatment processes," *IEEE Trans. Control Syst. Technol.*, vol. 27, no. 4, pp. 1480–1491, Jul. 2019.
[29] A. Mohammadzadeh, S. Ghaemi, O. Kaynak, and S. Khanmohammadi, "Robust H_∞-based synchronization of the fractional-order chaotic systems by using new self-evolving nonsingleton type-2 fuzzy neural networks," *IEEE Trans. Fuzzy Syst.*, vol. 24, no. 6, pp. 1544–1554, Dec. 2016.
[30] F. F. M. El-Sousy and K. A. Abuhasel, "Self-organizing recurrent fuzzy wavelet neural network-based mixed H_2/H_∞ adaptive tracking control for uncertain two-axis motion control system," *IEEE Trans. Ind. Appl.*, vol. 52, no. 6, pp. 5139–5155, Nov./Dec. 2016.
[31] K. Subramanian and S. Suresh, "A metacognitive sequential learning algorithm for neuro-fuzzy inference system," *Appl. Soft Comput.*, vol. 12, no. 11, pp. 3603–3614, 2012.
[32] J. Rong *et al.*, "A novel metacognitive fuzzy-neural model with backstepping strategy for adaptive control of uncertain nonlinear systems," *Neurocomputing*, vol. 230, pp. 332–344, 2017.
[33] B. Scholkopf and A.-J. Smola, *Learning With Kernels*. Cambridge, MA, USA: MIT Press, 2002.
[34] H. Hoffmann, "Kernel PCA for novelty detection," *Pattern Recognit.*, vol. 40, no. 3, pp. 863–874, 2007.
[35] M. Chen, P. Shi, and C. Lim, "Adaptive neural fault-tolerant control of a 3-DOF model helicopter system," *IEEE Trans. Syst., Man, Cybern., Syst.*, vol. 46, no. 2, pp. 260–270, Feb. 2016.
[36] H. Akagi, Y. Kanazawa, and A. Nabae, "Instantaneous reactive power compensators comprising switching devices without energy storage components," *IEEE Trans. Ind. Appl.*, vol. IA-20, no. 3, pp. 625–630, May 1984.
[37] J. Mindykowski, X. Xu, and T. Tarasiuk, "A new concept of harmonic current detection for shunt active power filters control," *Measurement*, vol. 46, pp. 4334–4341, 2013.
[38] S. Hou, J. Fei, Y. Chu, and C. Chen, "Experimental investigation of adaptive fuzzy global sliding mode control of single-phase shunt active power filters," *IEEE Access*, vol. 7, pp. 64442–64449, 2019.
[39] S. Hou and J. Fei, "Adaptive fuzzy backstepping control of three-phase active power filter," *Control Eng. Pract.*, vol. 45, pp. 12–21, 2015.
[40] Y. S. Lu and J. S. Chen, "Design of a global sliding-mode controller for a motor drive with bounded control," *Int. J. Control*, vol. 62, no. 5, pp. 1001–1019, 1995.
[41] R. Wai, J. Yao, and J. Lee, "Backstepping fuzzy-neural-network control design for hybrid maglev transportation system," *IEEE Trans. Neural Netw. Learn. Syst.*, vol. 26, no. 2, pp. 302–317, Feb. 2015.
[42] X. Zhao, P. Shi, and X. Zheng, "Fuzzy adaptive control design and discretization for a class of nonlinear uncertain systems," *IEEE Trans. Cybern.*, vol. 46, no. 6, pp. 1476–1483, Jun. 2016.
[43] H. Wang, P. Shi, H. Li, and Q. Zhou, "Adaptive neural tracking control for a class of nonlinear systems with dynamic uncertainties," *IEEE Trans. Cybern.*, vol. 47, no. 10, pp. 3075–3087, Oct. 2017.
[44] Q. Xu, "Continuous integral terminal third-order sliding mode motion control for piezoelectric nanopositioning system," *IEEE/ASME Trans. Mechatron.*, vol. 22, no. 4, pp. 1828–1838, Aug. 2017.

Shixi Hou received the B.S. degree in automation from Hohai University, Nanjing, China, in 2011, and the Ph.D. degree in electrical engineering from Hohai University, Nanjing, China, in 2016.

He is currently a Lecturer with Hohai University, Nanjing, China. His research interests include power electronics, adaptive control, nonlinear control, and intelligent control.

Juntao Fei (M'03–SM'14) received the B.S. degree in electrical engineering from the Hefei University of Technology, Hefei, China, in 1991, the M.S. degree in electrical engineering from the University of Science and Technology of China, Hefei, China, in 1998, and the M.S. and Ph.D. degrees in mechanical engineering from the University of Akron, Akron, OH, USA, in 2003 and 2007, respectively.

He was a Visiting Scholar with the University of Virginia, Charlottesville, VA, USA from 2002 to 2003. He was an Assistant Professor with the University of Louisiana, Lafayette, LA, USA from 2007 to 2009. He is currently a Professor with Hohai University, Nanjing, China. His research interests include power electronics, adaptive control, nonlinear control, intelligent control, dynamics and control of MEMS, and smart materials and structures.